HHS Public Access

Author manuscript

Adv Mater. Author manuscript; available in PMC 2024 April 01.

Published in final edited form as:

Adv Mater. 2023 April ; 35(15): e2207742. doi:10.1002/adma.202207742.

Self-healing, Reconfigurable, Thermal-switching, Transformative Electronics for Health Monitoring

Li Yang[*],
State Key Laboratory of Reliability and Intelligence of Electrical Equipment, School of Health Sciences and Biomedical Engineering, Hebei University of Technology, Tianjin 300130, China

Zihan Wang,
State Key Laboratory for Reliability and Intelligence of Electrical Equipment, Hebei Key Laboratory of Smart Sensing and Human-Robot Interaction, School of Mechanical Engineering, Hebei University of Technology, Tianjin 300401, China

Hao Wang,
State Key Laboratory of Polymer Material Engineering, College of Polymer Science and Engineering, Sichuan University, Chengdu 610065, China

Biqiang Jin,
State Key Laboratory of Polymer Material Engineering, College of Polymer Science and Engineering, Sichuan University, Chengdu 610065, China

Chuizhou Meng,
State Key Laboratory for Reliability and Intelligence of Electrical Equipment, Hebei Key Laboratory of Smart Sensing and Human-Robot Interaction, School of Mechanical Engineering, Hebei University of Technology, Tianjin 300401, China

Xue Chen,
State Key Laboratory of Reliability and Intelligence of Electrical Equipment, Key Laboratory of Bioelectromagnetics and Neuroengineering of Hebei Province, School of Electrical Engineering, Hebei University of Technology, Tianjin 300130, China

Runze Li,
State Key Laboratory of Reliability and Intelligence of Electrical Equipment, Key Laboratory of Bioelectromagnetics and Neuroengineering of Hebei Province, School of Electrical Engineering, Hebei University of Technology, Tianjin 300130, China

He Wang,

yangli5781@126.com, wujinrong@scu.edu.cn, huanyu.cheng@psu.edu.

Author Contributions

L.Y., J.W., and H.C. initiated the project. L.Y., C.M. and S.G. supervised the studies. L.Y. Z.W. and X.C. led the experiments and collected the overall data. Z.W., M.X. and Z.Z. contributed to the system development, fabrication, and characterization. Z.W. and R.L. performed the electronic circuit design and test. H.W., B.J., and Z.W. contributed to preparation and characterization of self-healing films. L.Y., Z.W., H.W., and H.C contributed to data analysis and cowrote the paper. All authors provided feedback on the manuscript.

Supporting Information

Supporting Information is available from the Wiley Online Library or from the author.

Conflict of Interest

The authors declare no conflict of interest.

State Key Laboratory of Polymer Material Engineering, College of Polymer Science and Engineering, Sichuan University, Chengdu 610065, China

Mingyang Xin,
State Key Laboratory of Reliability and Intelligence of Electrical Equipment, School of Health Sciences and Biomedical Engineering, Hebei University of Technology, Tianjin 300130, China

Zeshang Zhao,
State Key Laboratory for Reliability and Intelligence of Electrical Equipment, Hebei Key Laboratory of Smart Sensing and Human-Robot Interaction, School of Mechanical Engineering, Hebei University of Technology, Tianjin 300401, China

Shijie Guo,
State Key Laboratory for Reliability and Intelligence of Electrical Equipment, Hebei Key Laboratory of Smart Sensing and Human-Robot Interaction, School of Mechanical Engineering, Hebei University of Technology, Tianjin 300401, China

Jinrong Wu*,
State Key Laboratory of Polymer Material Engineering, College of Polymer Science and Engineering, Sichuan University, Chengdu 610065, China

Huanyu Cheng*
Department of Engineering Science and Mechanics, The Pennsylvania State University, University Park 16802, USA

Abstract

Soft, deformable electronic devices provide the means to monitor physiological information and health conditions for disease diagnostics. However, their practical utility is limited due to the lack of intrinsical thermal switching for mechanically transformative adaptability and self-healing capability against mechanical damages. Here, we report the design concepts, materials and physics, manufacturing approaches, and application opportunities of self-healing, reconfigurable, thermal-switching device platforms based on hyperbranched polymers and biphasic liquid metal. The former provides excellent self-healing performance and unique tunable stiffness and adhesion regulated by temperature for the on-skin switch, whereas the latter results in liquid metal circuits with extreme stretchability (> 900%) and high conductivity (3.40×10^4 S cm^{-1}), as well as simple recycling capability. Triggered by the increased temperature from the skin surface, a multifunctional device platform can conveniently conform and strongly adhere to the hierarchically textured skin surface for non-invasive, continuous, comfortable health monitoring. Additionally, the self-healing and adhesive characteristics allow multiple multifunctional circuit components to assemble and completely wrap on 3D curvilinear surfaces. Together, the design, manufacturing, and proof-of-concept demonstration of the self-healing, transformative, and self-assembled electronics open up new opportunities for robust soft deformable devices, smart robotics, prosthetics, and Internet-of-Things, and human-machine interfaces on irregular surfaces.

Graphical Abstract

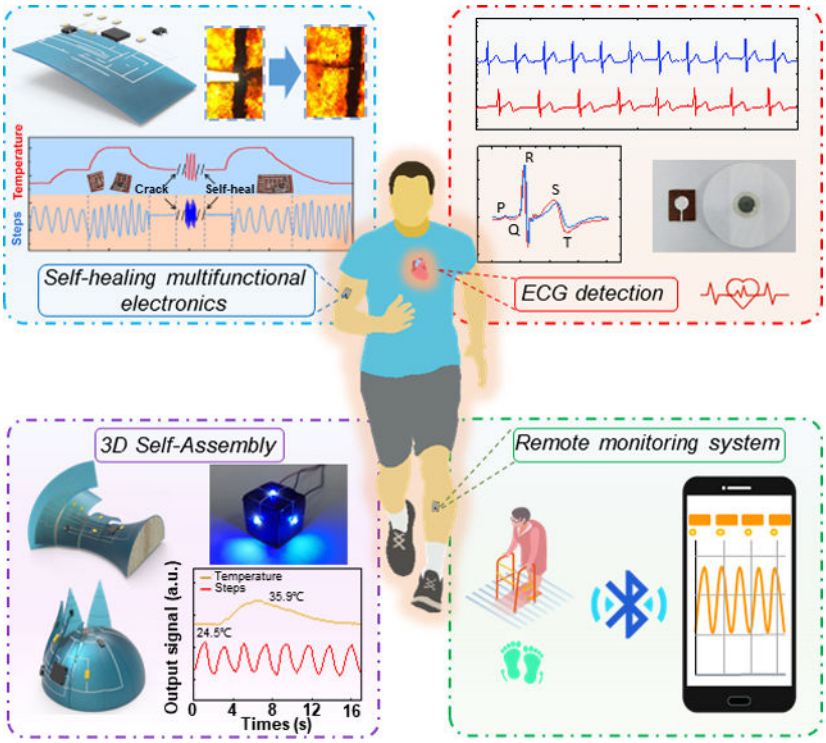

Printing solid-liquid biphasic liquid metal patterns on the hygroscopic hyperbranched polymer substrate demonstrates a self-healing, reconfigurable device platform with thermal-switching stiffness and adhesion. Triggered by the increased temperature, the device platform conformed and adhered to the textured skin or other 3D curvilinear surfaces can provide an integrated remote monitoring system for non-invasive, continuous, long-term health monitoring of people and structures.

Keywords

self-healing film; liquid metal printed circuits; multifunctional electronic device; thermal-switching; transformative characteristics; 3D conformal self-assembly

1. Introduction

The unique mechanical and electrical properties of the advent of flexible electronic devices allow their use in soft robots,[1,2] flexible sensors,[3,4] and flexible printed circuit boards (PCBs).[5,6] In particular, the skin-interfaced soft wearable electronics can monitor vital physiological data for early disease diagnostics,[7,8] effective in-time treatment,[9,10] and human-computer interfaces,[11,12] as well as provide electronic skin[13,14] to detect heat stress. However, these soft and flexible devices are inevitably susceptible to mechanical damage and failure from external friction, torsion, tear, and compression, presenting challenges for their long-term use in harsh environments. As a result, the bio-inspired self-healing materials (e.g., hydrogels,[15–17] dynamic covalent bonds,[18,19] supramolecular networks,[20,21] metal coordination bonds[22,23] have been used to fabricate self-healing

biosensors,[24,25] supercapacitors,[26,27] batteries,[28,29] and triboelectric nanogenerators.[30,31] Although the representative gel-based self-healing devices exhibit rapid healing, they suffer from poor thermal stability, mechanical strength, and healing repeatability. Creating conductive microchannel inside the self-healing material provides stable circuit connections and high repeatable healing, but the fabrication process for high-resolution microchannels is often complicated. As an alternative, directly printing flexible circuits based on polymer,[32,33] carbon-based materials[34,35] or liquid metals on the self-healing substrate is attractive. Besides high fluidity, conductivity, and stimulus-responsive properties to external light or thermal,[36,37] liquid metals can also self heal. The commonly used gallium-based liquid metal such as eutectic gallium-indium alloy (eGaIn) exhibits a high tensile range and thermal conductivity (= 26.6 W m^{-1} K^{-1}),[38] low melting temperature (M_p < 15.5°C),[39] low toxicity, and simple processing capability. The thin oxide layer (ca. 3 nm)[40] rapidly formed on the outside surface of eGaIn also helps maintain mechanical stability but results in high surface tension (~600 mN m^{-1})[41] and poor adhesion create challenges in printing. Efforts to improve printability include laser sintering,[42,43] electrowetting,[44] microchannels,[45] 3D printing,[46] and metal doping.[47–49] However, it is still challenging to maintain high electrical performance in the printed circuits, provide easy integration with Commercial-Off-The-Shelf (COTS) components,[50,51] and recycle electronics to minimize e-waste for reduced health and environmental issues.[52,53]

While the soft deformable devices with strong adhesion to the skin device are often desirable for high-fidelity continuous monitoring, the ones with high mechanical strength can provide a stable configuration for robust operation in off-body applications. Therefore, transformative devices are highly desirable for use in different application scenarios. The self-healing property can further improve mechanical robustness even against damages. The conformal electronics transferred to 3D complex surfaces may experience local bulking and cracking to result in changes in the output signals and even failures in electronic devices.[54,55] Therefore, it is possible to combine reconfigurable modular electronic system[56,57] with the kirigami design concept and self-healing materials[58] to conveniently assemble multiple two-dimensional (2D) components on three-dimensional (3D) curvilinear surfaces.

Here, we introduce a self-healing, thermal-switching, transformative multifunctional electronic device platform based on printable biphasic Ga-In (bGaIn) and self-healing hygroscopic randomly hyperbranched polymers (HRHP). The new self-healing HRHP provided excellent self-healing performance and, more importantly, unique tunable stiffness and adhesion regulated by temperature for the on-skin switch. The reliable connection between the bGaIn circuit and COTS components (e.g., micro thermometer and accelerometer) easily results in the proof-of-concept demonstration to measure vital physiological signals such as electrophysiology, temperature, and motion. The hydrogen bond exchange reaction in the polymer network of HRHP and the fluidity of the liquid phase in bGaIn allow the resulting electronic devices to quickly heal from fracture and restore electrical performance at room temperature. The HRHP electronics can be conveniently switched between rigid and soft modes by temperature to exhibit variable stiffness for use in versatile applications. The COTS components and bGaIn circuits can also be recycled with an ethanol solution for reuse. Moreover, combining the self-healing bGaIn/HRHP with

kirigami design results in conformal assembly of multiple 2D components on 3D curvilinear surfaces.

2. Results

2.1 Design and Fabrication for Multifunctional, Thermal-Switching Transformative Electronics

The fabrication of bGaIn circuits on the HRHP substrate through a mask printing method allows facile integration of the COTS electronic components, where a thin HRHP film (ca. 500 μm thick) also serves as an insulation layer at the intersection of bGaIn traces (Figure 1a,b,c). The method provides a simple and efficient manufacturing approach for the demonstrated self-healing, reconfigurable, thermal-switching, transformative electronic devices for health monitoring, intelligent robotics, the Internet-of-Things, and flexible human-machine interfaces. In brief, randomly hyperbranched polymers (RHP) were synthesized by one-pot Michael addition between *N,N'*-methylene diacrylamide (MBA) and 1,4-butanediamine (BDA) at a molar ratio of 1:1 due to the reaction between -NH- of BDA and CH_2=CH- on MBA under a mild condition (30°C, 24 h) (Figure S1a).[59] The tertiary and secondary amines generated by Michael addition serve as branching points and chain-extending units, respectively. Since each -NH- of BDA can react with CH_2=CH- on MBA and the mole ratio of the former to the latter changes from 9:4 to 7:4, the resulting RHP molecule ends with primary amine (Figure S1b). HRHP was obtained after the water uptake of RHP is about 10%. HRHP is a random hyperbranched polymer with 3D spatial molecular configuration, which has abundant and highly mobile external branching units and end groups.[59] Besides high-density multiple hydrogen bonds formed between primary amine terminals, amide groups, and secondary amines on branched chains, the randomly branched structure of HRHP prevents the ordered packing of the molecules to provide “free” moieties. When the two damaged sections of HRHP are brought into contact, the free moieties can exchange with the associated hydrogen bonds (Figure S2) and result in self-healing at room temperature with strong mechanical strength (Figure S3). Our previous work also provides the evidence for instant self-healing with a tensile stress of 5.5 MPa recovered within 1 minute after the fracture-healing cycle at room temperature (without external force).[59] The excellent wettability of bGaIn can firmly connect the pins of COTS components without welding or soldering (Figure S4 and S5). The self-healing of HRHP relies on hydrogen bonds to heal the fractured substrate segments and the bGaIn lines bonded on the HRHP reconnect to restore stable electrical connection while still exhibiting excellent flexibility, which is difficult to achieve with alternative materials (Figure 1d). The self-healing property is needed for both bGaIn circuits and the substrate to yield a fully self-healing electronic device. As the bGaIn and COTS components are readily separated from the HRHP with simple ethanol immersion, they can be recycled and reused for new functional devices to lower production costs and promote environmentally green electronics (Figure 1e).

2.2 Material Characterization of The HRHP Films and bGaIn

The RHP can absorb water from the air and thus becomes softened and easier to handle, compared with the pristine material. After placing the RHP sample in a petri dish at 30%

relative humidity (RH) for one month, the water uptake of RHP is about 10%, as determined by comparing its thermal gravimetric analysis (TGA) curve with that of the “dry” RHP (Figure 2a and Figure S6). The contact angle of the water droplet on the hygroscopic HRHP film decreases from 118.5° to 58.9° over the contact of 20 min (Figure S7). The glass transition temperature (T_g) measured by differential scanning calorimetry (DSC) is 9°C for the HRHP, with the second transition at ca. 80°C attributed to the loss of water (Figure 2b). This T_g enables the material to readily respond to temperature and switch between rigid and soft modes. Interestingly, the hydrogen bonds of the HRHP basically remains the same as those of the pristine materials, as revealed by Fourier transform infrared spectroscopy (FTIR) (Figure 2c). The characteristic peaks at 1648 cm^{-1} and 1540 cm^{-1} are assigned to the hydrogen-bonded amide I and II bands, respectively. Moreover, these two peaks are very broad, indicating the coexistence of multiple hydrogen bonds and “free” amide and -NH- groups in the HRHP molecules. As the temperature increases from 30 to 150°C, the amide I and II (“free” amide groups) bands are shifted toward high and lower wavenumbers, respectively, indicating gradual dissociations of the hydrogen bonds. Temperature-dependent ^1H nuclear magnetic resonance spectroscopy (^1H NMR) in the previous work[59] also confirms the dynamic characteristics of hydrogen bonds (-NH-, -NH_2-) at room temperature with the shifted proton peaks. According to Noda’s rule in the 2D correlation analysis of -NH- vibration in FTIR spectra, free amino and amide groups are more active in the temperature range around T_g, and free -NH- moieties move and exchange with the moieties associated with hydrogen bonds to complete the healing of polymer.[59] The dynamic nature of the hydrogen bonds imparts the HRHP with high self-healing ability, as demonstrated in the stress-strain curves over 10 consecutive cutting-healing cycles (Figure S8a) or under different RH levels (i.e., 20%, 50%, and 80%) (Figure S8b). Although the healing strength of HRHP gradually decreases with the increasing RH, the flexibility is increased due to moisture absorption.

To discuss the effect of laser ablation on HRHP film, the film surface before and after ablation was observed by scanning electron microscope. The surface of HRHP film has obvious boundaries before (left) and after (right) laser ablation (Figure 2e). After fivefold magnification, the left half of the film surface is still very smooth (Figure 2d), while the right half is rough and many granular substances appear (Figure 2f). The measurement shows that the film thickness after laser ablation was reduced by about 60 μm, which is because the high heat of the CO_2 laser melts the surface of HRHP film, then the polymer material was cooled after melting to form a surface with high viscosity and a small part of the polymer was sintered into small particles at high temperatures at the same time. Therefore, CO_2 laser ablation becomes a favorable factor to improve the surface adhesion of HRHP films. As can be seen from the SEM image (Figure 2g), bGaIn consists of a solid phase and a liquid phase. The solid phase is partially embedded in the liquid phase and tightly wrapped by the liquid, forming a state of biphasic coexistence. The energy dispersive spectrum of bGaIn shows that the concentration of oxygen and gallium in the solid particle region is higher than that in the liquid region (with vanishing In) to indicate the formation of solid Ga_2O_3 particles from the oxidation of Ga (Figure 2h). It is worth noting that the electron beam may also change the phase of GaIn, so a more accurate and quantitative measurement may be needed to confirm the result. There is no obvious peak in the X-ray

diffraction pattern of the bGaIn, which indicates that bGaIn does not contain crystals (Figure 2i). This is because the temperature of whole manufacturing process of bGaIn is far lower than the crystallization temperature (~350°C)[60] of the oxidation product: Ga_2O_3, resulting in the amorphous state of Ga_2O_3.

2.3 Mechanical and Thermal Properties of The Mechanically Transformative HRHP Films

Actuated by the temperature, the HRHP film exhibits variable stiffness characteristics and can be switched from rigid to flexible states (Figure 3a). The flat HRHP film with high stiffness can easily bear a weight of 50 g and maintain the specific shape upon loading, leading to easy insertion into soft jelly. On the other hand, the flexible HRHP film with low stiffness bends under its own gravity and can not bear the weight, with a soft characteristic to deform onto the jelly surface. The temperature-dependent stiffness change of HRHP can be easily visualized by first freezing the HRHP film to −2°C for 10 minutes and then slowly raising the temperature to room temperature. With a 10 g weight placed on one end of the horizontal HRHP film clamped to a tweezer on the other end, the level of bending directly reflects the stiffness change. As confirmed by the infrared images, the slight bending at 9.5°C becomes more drastic at 10.2°C resulting in the falling of the weight (Figure S9). The direct measurement of the modulus change at two temperature values also shows a significant modulus reduction from 294.69 MPa in the rigid state to 0.15 MPa in the flexible state (Figure 3b). The bending rigidity of the HRHP substrate is reduced from 1272.09 $N{\cdot}mm^2$ to 133.94 $N{\cdot}mm^2$ as it switches from the rigid to flexible state (Figure S10). Further evaluation of the mechanical properties relies on the measured stress-strain curve of the flexible and rigid states at 25°C and 5°C, respectively (Figure 3c). Compared to the commonly used polydimethylsiloxane (PDMS) and Ecoflex with a modulus of 0.89 MPa and 0.04 MPa (measured at 25°C), the elastic modulus of 0.15 MPa for the flexible HRHP is in between the two, whereas that of 294.69 MPa for the rigid HRHP is much higher (Figure S11). While the elongation at fracture of 56.38% for the rigid HRHP is much smaller, 197.63% for the soft HRHP is also in between 99.29% for PDMS and 349.28% for Ecoflex. The temperature-driven variable stiffness of the HRHP is attributed to the change from a rigid glassy state at a lower temperature to a rubbery state at a higher temperature due to enhanced movements of molecules and moieties. The unique characteristic of tunable modulus enables HRHP electronic devices to maintain flexible conformal and adhesive attachment on the warm skin surface for continuous real-time monitoring of health-relevant signals. Meanwhile, the high mechanical strength in low-temperature allows for easy handling and manipulation (to avoid damage by excessive forces) in off-body applications.

In addition to the increased compliance, the flexible HRHP film also exhibits excellent adhesion to diverse surfaces, including paper, cotton fiber, plastic, glass, metal, and skin (Figure S12). Compared with PDMS and Ecoflex, the adhesion of 7.3 $N\ m^{-1}$ for the flexible HRHP film measured by a tensile strength testing platform (Figure S13) is higher. The adhesion can be further increased by another ca. 5 times to 37 $N\ m^{-1}$ when processed with CO_2 laser ablation (Figure 3d). The stable adhesion relies on molecular bond exchange and recombination when the HRHP polymer is brought into contact with other materials. Melting of the the initially smooth surface of the HRHP film by the laser spot at a

high temperature (>> T_g) increases the molecular activity and thermal motion energy for enhanced molecular bonding ability.[61] The created rough surface with high viscosity after ablation also contributes to the improved adhesion. The reduced adhesion from body/room temperature drastically reduces to 0.65 N m^{-1} at a low temperature (1.9°C) (Figure 3e) due to the rigid characteristics of the polymer.

Therefore, local heating before the function can firmly adhere the device to the skin (Movie S1) and allows a gentle removal of electronics from the skin by decreasing the temperature without damaging the soft surface or skin (Figure 3f). The strong adhesion of the flexible HRHP film to the skin also does not result in adverse effects even after one week of use (Figure 3g), supporting its excellent durability for practical applications. Excellent biocompatibility of HRHP is also confirmed by the cell viability of NIH 3T3 fibroblasts measured by the CCK-8 assay (on the 1^{st}, 4^{th}, and 7^{th} day) and the absence of allergy or discomfort after attaching HRHP to the skin for 24 hours (Figure S14).

2.4 Fabrication and Electromechanical Characterizations of The Stretchable bGaIn Circuits

After ultrasonic mixing of GaIn with ethanol, the liquid metal particles exhibit the highest volume percentage of 27.5% in the range of 2.2~3.2 μm. The volume- and surface-weighted mean diameters are 5.52 and 3.05 μm, respectively (Figure S15). Spraying the GaIn particle ink mixed with ethanol on the Si wafer, followed by rapid evaporation of ethanol at 90°C, creates bGaIn with the upper layer of the film oxidized to form Ga_2O_3 and the lower layer in the liquid phase. Multilayered films from repeated spraying can then be scraped off from the Si wafer to yield the biphasic GaIn alloy (bGaIn) paste (Figure 4a). The contact angle of 46.3° for bGaIn on HRHP is much smaller than that of 142.9° for GaIn, indicating significantly improved wettability (Figure S16). When squeezing the bGaIn with a thin film applicator, the solid phase of the bGaIn is partially ruptured and the liquid phase is then printed through a shadow mask to form a conductive pattern on a variety of substrates (e.g., Very High Bond (VHB) tape and kraft paper) (Figure 4b). The letter “H” printed on the surface of the latex balloon remains intact even after the balloon volume is increased by three times. The printing of delicate bGaIn patterns is also compatible with porous cotton textiles. The patterned bGaIn circuits on diverse substrates (e.g., glass, printing paper, latex gloves, sandpaper, and cotton fiber) (Figure S17) with respective surface roughness (defined as the average deviation in the surface profile) demonstrate excellent printability (Figure S18). Additionally, the highly stretchable bGaIn on the VHB tape provides a stable electrical connection even after a tensile strain of 200%, as evidenced by the bright LED array with a “HEBUT” (Hebei University of Technology) pattern (Figure 4c).

Evaluation of the electromechanical properties of the bGaIn is characterized by the normalized resistance change (R/R_0) of bGaIn traces with a dog bone pattern (16 × 1 mm) on VHB tape under uniaxial tensile strain. The bGaIn traces exhibit a highly stable electrical performance, with R/R_0 to be 1.25 (Figure S19), 3, and 14 at a tensile strain of 100%, 300%, and 940%, respectively (Figure 4d). These values are smaller than the theoretical predictions (4/16/108 at 100/300/940%) of the bulk liquid metal conductor according to Pouillet’s law: [62], where is the applied strain. The electromechanical performance of bGaIn traces is also

stable over 2,000 cycles for a cyclic tensile strain to 100% (Figure S20) and 300% (Figure 4e). Although the resistance of the bGaIn circuit is affected by the temperature, it only fluctuates by 9% as the temperature increases from −10 to 100°C (Figure S21), due to more active atoms in bGaIn reducing the movement of electrons. In summary, the printed bGaIn with high initial conductivity of 3.40×10^4 S cm^{-1}, remarkable extensibility (> 940%), stability over a wide temperature range, and low resistance change under large tensile strains compares favorably over the other stretchable conductors[63–72] (Figure 4f and Table S1). As the printed bGaIn is almost incompressible, stretching-induced elongation in the trace length decreases the thickness and width of the liquid phase, resulting in emergence of the solid phase to the surface and the increased resistance. After the stretching is removed, the solid part is remixed with the liquid part (Figure S22). The biphasic structure of bGaIn can maintain a stable electrical performance with high wettability and continuity during stretching due to the connected liquid phase underneath the solid phase. The high wettability of the liquid phase also ensures excellent adhesion to the solid phase and the substrate during the stretching process.

2.5 Multifunctional Sensing System for Human Health Monitoring

Printing the circular bGaIn pattern (radius of 4mm) on the HRHP substrate provides the biocompatible electrode to measure the electrophysiological signals such as the electrocardiogram (ECG). With the commercial Xinweilai ECG sensing kit, the ECG measured with the bGaIn-HRHP electrodes in a two-lead configuration placed on the chest (Figure S23) compares excellently with that from the commercial Ag/AgCl electrodes (Figure 5a). The characteristic P, Q, R, S, and T peaks are almost identical to these two types of electrodes, with the P wave, QRS complex, and T wave corresponding to the activation of the atria, activation and depolarization of the ventricles, and repolarization of the ventricles, respectively.[73] Although the bGaIn-HRHP electrodes (3.5 cm^2) have a much smaller contact area than the Ag/AgCl electrodes (21.2 cm^2), the signal-to-noise ratio (SNR) defined as $SNR(dB) = 20\log\frac{V_{rmsi}}{V_{rmsn}}$ (with and representing the root mean square value of the ECG signals without and with noise)[74] of 45.27 dB is still higher than that of Ag/AgCl electrodes (30.82 dB).

The firmly adhered bGaIn-HRHP electrodes on the skin of the chest provide convenient means to measure the ECG signals before, during, and after exercise. The heart rate of the human subject increases from 80 beats/minute at rest to 120 beats/minute after running for 10 minutes (Figure 5b). In addition, a high SNR of > 45 dB is well maintained at different skin RH levels (e.g., 40% RH at rest, 60% RH from slight sweating, and 80% RH from significant sweating) (Figure S24a, b) and temperatures (e.g., 25°C, 35°C, and 45°C) (Figure S24c, d). As the autonomic nervous system regulates the cardiac sinoatrial node, the heart rate before and after exercise (Figure 5c) and heart rate variability determined from the R-to-R and P-to-P peak intervals (Figure S25) are accurately recorded to diagnose autonomic nervous dysfunction. The dynamic ECG measurements during exercise show a slightly decreased heart rate from walking to standing (Figure 5d). Deep breathing is associated with increased pulmonary blood flow and decreased cardiac blood flow, resulting

in a significant upward shift in measured R peaks and a downward shift in the measured S peaks (Figure 5e).

Although the ECG measured by the fractured bGaIn-HRHP electrodes exhibits a reduced SNR from 46.22 to 22.26 dB, the self-healed HRHP electrodes at room temperature are able to recover the ECG signals with an slightly reduced SNR value of 44.67 dB compared with the pristine electrodes (~3.6%) (Figure 5f,g). In addition, the measured ECG signals from the bGaIn-HRHP electrode during elbow bending, chest squeezing, and stretching (Figure 5h) all exhibit higher SNR values than those from the commercial Ag/AgCl electrodes (Figure 5i). Printing a circular Ag pattern on the HRHP substrate also prepares the Ag-HRHP electrode with high conductivity and SNR (> 30 dB) upon fracture-healing and various mechanical deformations. Although the SNR from the Ag-HRHP electrode is higher than that of commercial Ag/AgCl electrodes, it is much smaller than that of the bGaIn-HRHP electrode (> 45 dB) (Figure S26), due to the less conformal contact with the skin.

The integration of the bGaIn circuits with COTS components on the self-healing HRHP provides a simple solution to conveniently measure the skin peripheral temperature and varying motions (Figure 6a, b). The measured temperatures at the low, medium (room), and high temperature settings (red line) agree reasonably well with those from the commercial thermometer. The acceleration change measured from the arm distinguishes various exercise states, including walking, jogging, and resting (blue line). When walking, the blue line presents a regular waveform similar to a sine wave, because the arm swings gently and slowly at this time. During jogging, the swing speed of the arm is accelerating while the amplitude is irregular, and the waveform becomes compact. At rest, the arm stops swinging and the waveform becomes a straight line. The discontinued data (e.g., temperature and motion) due to the circuit damage (e.g., cut by a blade) can resume after the device self heals (by connecting two circuit fragments) at room temperature. The self-healing process takes ca. 5 minutes to recombine a large number of hydrogen bonds and reconfigure the network in hyperbranched polymers, with the incision becoming almost invisible to the naked eye (Figure 6c). This excellent instantaneous self-healing performance at room temperature is superior to most self-healing materials, including polyurethane,[75,76] histidine elastomer,[77] multiblock-copolymer,[78] and others. The self-healing property allows the fractured surface in the device (that often occurs in practical applications) to rapidly “revive” and recover the designed properties and functions, which can improve mechanical robustness and the service life of the resulting electronic electronics. In addition, the multifunctional HRHP electronics also exhibit excellent stability over a wide temperature range from −10 to 80°C (Figure S27). The changes in the output signals from HRHP electronics switched from flexible to rigid state before and after healing is negligible, with a fluctuation of only 1.85% in the background noise (Figure S28). The mechanical deformations such as stretching and bending show negligible effects on HRHP electronics on the skin, as evidenced by the fluctuation of 2.79% in the root mean square of the signal background noise: 0.0698 for no loading, 0.0718 for 30% tensile strain (the maximum deformation of human skin),[79] and 0.0700 for bending (bending radius of 10 mm) (Figure S29).

The liquid metal and electronic components can also be recycled for reuse (Figure 6d). In brief, soaking and stirring the circuit with a glass rod in ethanol for 10 minutes to separate the electronic components and liquid metal from the HRHP film. Drying the collected liquid metal and electronic components in a drying oven at 50°C for 10 minutes completely evaporates the ethanol, resulting in the recycled bGaIn and electronic components for reuse. The resistance of the recycled bGaIn is within 0.5% of the initially prepared ones (Figure 6e), whereas the recycling process can also be repeated multiple times with almost no changes in the resulting devices. The newly prepared device platform with the recycled bGaIn and electronic components can accurately detect the temperature and motion (Figure 6f).

2.6 Remote Monitoring System and Conformal Electronics Based on Self-Healed Kirigami Assembly

It is of significant interest to wirelessly monitor the physical conditions of the elderly in real-time for healthy aging. By connecting the HRHP electronics with a micro PCB, the motion signals of the elderly can be wirelessly communicated to the smart phone APP via Bluetooth for the medical professionals to quickly respond to anomalous situations such as falls and shivers (Figure 7a). After converting the output signals from the COTS accelerometer in HRHP electronics into voltage values through a voltage divider, followed by amplification, the data are processed by a low-pass filter to remove the noise and then by a 16-bit analog-to-digital converter for transmission to the microcontroller. The microcontroller wirelessly transmits the digital signals via Bluetooth to be displayed on the smartphone APP in real-time (Figure 7b,c, see the schematic diagram in Figure S30). The robust attachment of the integrated wireless monitoring system on the arm provides stable acquisition of motion signals from human subjects over various activities such as walking and running. The detection of unintentional falls down the stairs allows medical professionals to give prompt attention for preventing the deterioration of the elderly (Movie S2).

The self-healing and strong adhesion properties of HRHP films can also be combined with kirigami assembly to prepare conformal electronics on 3D curvilinear surfaces, including a cubic LED circuit (Figure S31) and multifunctional circuits on the saddle and hemispherical surfaces. The shape of each part designed by the 3D modeling and surface expansion method with the circuit designed by projection onto the 2D plane of each part provides the device on the saddle surface (Figure 7d,e). As for the device on the hemispherical surface, each petal component with determined length and height at the bottom edge is then designed to have two arc sides, with the distance from the side to the centerline corresponding to the divided circumference of the spherical surface at each height (Figure 7f, g). Next, cutting the HRHP into the designed shape for each part by the CO_2 laser is followed by printing of the bGaIn circuit through a shadow mask. After conforming and adhering the flexible HRHP onto the target 3D curvilinear surface, self-healing between adjacent parts at room temperature connects them to assemble the device on the 3D surface (Figure S32). The resulting device platform can accurately and reliably measure the temperature and motion from the deformable 3D curved surfaces (Figure 7h) with minimum changes compared

to their planar counterparts (Figure S33), demonstrating a high potential for the future intelligent Internet-of-Things.

3. Conclusion

In summary, this work reports the design, fabrication approaches, characterization, and demonstration of a self-healing, thermal-switching, mechanically transformative electronic device based on printed bGaIn and COTS components on the self-healing HRHP thin films. With variable stiffness and adhesion of the HRHP film, the device can strongly attach to the skin switched on by the temperature and conveniently removed by cooling. Besides self-healing from mechanical damages, the bGaIn and electronic components can be separated and recycled by soaking in ethanol for reuse to print circuits, detect temperature and motion. Moreover, the self-healing and strong adhesion properties can be combined with kirigami design and self-assembly to conveniently fabricate conformal electronics on the 3D curvilinear surfaces for smart Internet-of-Things and healthcare.

4. Experimental Section

Synthesis of hygroscopic randomly hyperbranched polymers (HRHP):

The synthesis of HRHP followed the protocols reported in our previous work.[59] *N,N'*-methylene diacrylamide (MBA, 99+%) and Methanol (99.9%) were purchased from Adamas. 1,4-Butanediamine (BDA, 98+%) was purchased from Alfa Aesar. Acetone and deionized water were purchased from Chengdu Kelong Chemical Reagent Factory. All the chemicals were used without further purification. The RHP were synthesized by a one-pot method through Michael's addition reaction between MBA and BDA with a molar ratio of 1/1. Specifically, MBA (0.08 mol) was added into a round bottom flask equipped with a magnetic stirrer containing a mixed solvent of 60 mL methanol and 30 mL deionized water at 30°C, followed by stirring until MBA was fully dissolved. Next, BDA (0.08 mol) was dissolved in a beaker containing a mixed solvent of 20 mL methanol and 10 mL deionized water, which was then directly fed into the flask. After stirring the mixture at 30°C for 24 h, the solution was poured into a beaker containing 1,000 mL acetone to precipitate at room temperature. The crude product was washed 5 times with acetone and then dried in a vacuum oven at 50°C for 48 h. The number-average molecular weight and weight-average molecular weight of RHP are 8091 and 16173 g mol^{-1}, respectively. The polydispersity index is 2.0. The degree of branching (DB) is 0.24, as determined by ^{13}C, ^{1}H-Heteronuclear Single Quantum Correlation (^{13}C, ^{1}H-HSQC), and quantitative ^{13}C NMR spectra.

After placing the rectangular mold (304 stainless steel) on the upper surface of the iron plate wrapped with tinfoil, ca. 1.1g RHP raw material was put into the mold and then the mold was covered with another iron plate wrapped with tinfoil. Hot-pressing under 10 MPa at 100°C for 30 min yielded the RHP film (e.g., 3.5 cm long, 2 cm wide, and 1 cm thick). HRHP was obtained by placing RHP in a petri dish at 30% RH for one month.

bGaIn preparation:

eGaIn (75.5% Ga, 24.5% In, Sigma Aldrich) of 90 mg was added to 1 ml of ethanol and then ultrasound for one hour in an ultrasonic homogenizer (SCIENTZ-IID) with 400W to

prepare liquid metal particle ink. The as-prepared ink of 1.5 ml was sprayed onto the silicon substrate using a spray gun to form a thin film, followed by drying at 90°C for 60 s to completely evaporate the ethanol. The spraying-drying process was repeated ten times to give a thick coating, which was then scraped off with a scraper to yield the printed bGaIn.

Electrical and mechanical characterizations:

The stress-strain curve, elastic modulus, and elongation at fracture of HRHP films in rectangular shapes (35 mm × 7 mm, 1 cm thick) were measured by a universal testing machine (Xinsansi, CMT6104). The adhesion between the test substrate and a glass slide was measured by progressively peeling one end of the substrate with a tensile strength tester away from the glass slide, with the temperature adjusted by the Peltier and radiator at the bottom.

The resistance of the dog-bone-shaped bGaIn pattern (16 mm × 1 mm) was measured using a four-point probe. The thickness of the sample was measured using a 3D optical profiler and averaged from five measurements. The roughness of the substrate surface was measured with a roughness meter (Shidaijiaxiang, TR200).

Fabrication of self-healing multifunctional electronics:

The paper mask was first prepared by cutting 0.1 mm-thick backing paper with a CO_2 laser (Universal Laser systems VLS 2.30, wavelength of 10.6 μm) in vector mode (power of 0.45 W, speed of 19.05 mm s^{-1}, image density of 500 PPI, defocus distance of 1.2 mm). After firmly fixing the paper mask on the substrate, pressing and smearing the bGaIn paste with a thin film applicator (Elcometer 3540) evenly filled the opening of the paper mask. Removing the backing paper mask left the bGaIn circuits on the HRHP thin-film substrate. Microelectronic components were then placed in the designed locations with the help of a magnifying glass. A small piece of thin HRHP film was used between intersecting lines to avoid short circuits. Connecting the self-healing multifunctional circuits to the external microcontroller (Arduino Mega 2560) using copper wires completed the fabrication. The temperature sensor MCP9700 relies on a linear thermistor to convert the temperature (in the range from −40 to 125°C with a measurement accuracy of 0.01°C) into analog voltage changes. The accelerometer ADXL335 with suspended polysilicon springs over a fixed conductive plate (built on top of the silicon chip) changes the measured capacitance with the applied acceleration to detect the acceleration in the range of ± 3g (g = 9.8 m s^{-2}).

Recycling process:

After completely immersing the self-healing multifunctional device in 25 ml ethanol (99%) in the beaker for 10 minutes, gently stirring with a glass rod helped bGaIn and electronic components delaminate from the HRHP substrate. Pouring out the ethanol allowed the collection of liquid metal and electronic components at the bottom of the beaker with tweezers. Placing them in the petri dish and drying them in a drying oven at 50°C for 10 minutes completely evaporated the ethanol, resulting in the recycled bGaIn and electronic components.

Characterization:

SEM images were taken by a field emission SEM (TESCAN, GAIA3). A D8 Advance (Bruker) X-ray diffractometer was used to measure XRD patterns. The uniaxial tensile strain was applied by a universal materials testing bench (JSV-H1000). The resistance of the bGaIn circuits was measured by a Keithley 2400 source meter.

Determination of biocompatibility:

All human subject studies were approved by The Pennsylvania State University (protocol number STUDY00009245). NIH 3T3 fibroblasts (Zhongqiaoxinzhou) were cultured in a complete growth media that comprised high glucose modified Eagle medium (DMEM) with L-glutamine, supplemented with 10% fetal bovine serum and 1% penicillin-streptomycin. [80] The cells were seeded into 96-well culture plates, maintained at 37°C in a humidified atmosphere in the presence of 5% CO_2. The first column of the 96-well culture plate was used as the control group. 0.001 g HRHP film was added into the second, third, and fourth columns on the 1st, 4th, and 7th day, respectively (five parallel samples in each group). After seven days, the culture medium was replaced by 100 μL fresh DMEM. 10 μL CCK-8 (Solarbio, LIFE SCIENCE) was then added to the control and HRHP groups. At last, the cell viability of NIH 3T3 was measured with a multimode plate reader (VICTOR Nivo, Perkin Elmer).

Supplementary Material

Refer to Web version on PubMed Central for supplementary material.

Acknowledgments

This work was supported by the National Natural Science Foundation of China (51705126, 61871173), the Key Research and Development Project of Hebei Province (20271701D, 22371703D), the Project funded by China Postdoctoral Science Foundation (2022M722378), and the Innovation Financing Program for Postgraduates of Hebei Province (CXZZSS2022052). H.C. acknowledges the support provided by NIH (Award Nos. R21EB030140, U01DA056242, and R61HL154215), NSF (Grant No. ECCS-1933072), and Penn State University.

Data Availability Statement

The authors declare that the main data supporting the findings of this study are available within the article and its Supplementary Information.

References:

[1]. Won P, Kim KK, Kim H, Park JJ, Ha I, Shin J, Jung J, Cho H, Kwon J, Lee H, Ko SH, Adv. Mater 2021, 33, 2002397.

[2]. Fu C, Xia Z, Hurren C, Nilghaz A, Wang X, Biosens. Bioelectron 2022, 196, 113690.

[3]. Yang L, Yi N, Zhu J, Cheng Z, Yin X, Zhang X, Zhu H, Cheng H, J. Mater. Chem. A 2020, 8, 6487.

[4]. Yang L, Ji H, Meng C, Li Y, Zheng G, Chen X, Niu G, Yan J, Xue Y, Guo S, Cheng H, ACS Appl. Mater. Interfaces 2022, 14, 17818. [PubMed: 35394746]

[5]. Cui J, Luo S, Ye F, Chen L, Appl. Phy. A 2021, 127, 666.

[6]. Singh S, Matsui H, Tokito S, Phys J. D: Appl. Phys 2022, 55, 135105.

[7]. Chen X, Li R, Niu G, Xin M, Xu G, Cheng H, Yang L, Chem. Eng. J 2022, 444, 136631.

[8]. Yang L, Zheng G, Cao Y, Meng C, Li Y, Ji H, Chen X, Niu G, Yan J, Xue Y, Cheng H, Microsyst. Nanoeng 2022, 8, 78. [PubMed: 35818382]

[9]. Chen G, Xiao X, Zhao X, Tat T, Bick M, Chen J, Chem. Rev 2022, 122, 3259. [PubMed: 34939791]

[10]. Wang Y, Yang B, Hua Z, Zhang J, Guo P, Hao D, Gao Y, Huang J, Phys J. D: Appl. Phys 2022, 55, 134001.

[11]. Yang L, Wang H, Yuan W, Li Y, Gao P, Tiwari N, Chen X, Wang Z, Niu G, Cheng H, ACS Appl. Mater. Interfaces 2021, 13, 60531. [PubMed: 34894673]

[12]. Wu W, Ren Y, Jiang T, Hou L, Zhou J, Jiang H, Chem. Eng. J 2022, 430, 132635.

[13]. Zeng X, Liu Y, Liu F, Wang W, Liu X, Wei X, Hu Y, Nano Energy 2022, 92, 106777.

[14]. García-Ávila J, Rodríguez CA, Vargas-Martínez A, Ramírez-Cedillo E, Martínez-López JI, Materials 2022, 15, 256.

[15]. Zheng C, Lu K, Lu Y, Zhu S, Yue Y, Xu X, Mei C, Xiao H, Wu Q, Han J, Carbohydr. Polym 2020, 250, 116905. [PubMed: 33049881]

[16]. Tie J, Rong L, Liu H, Wang B, Mao Z, Zhang L, Zhong Y, Feng X, Sui X, Xu H, Polym. Chem 2020, 11, 1327.

[17]. Xu W, Wang W, Chen S, Zhang R, Wang Y, Zhang Q, Yuwen L, Yang W, Wang L, Colloid Interface Sci J. 2021, 586, 601.

[18]. Fan P, Xue C, Zhou X, Yang Z, Ji H, Materials 2021, 14, 2680. [PubMed: 34065375]

[19]. Lu C, Yu C, Yeh YC, Acta Biomater. 2021, 130, 66. [PubMed: 34098090]

[20]. Zhang L, Wang D, Xu L, Zhang A, Polym. Chem 2021, 12, 660.

[21]. Wei H, Yang Y, Huang X, Zhu Y, Wang H, Huang G, Wu J, J. Mater. Chem A 2020, 8, 9013.

[22]. Shi Y, Wang M, Ma C, Wang Y, Li X, Yu G, Nano Lett. 2015, 15, 6276. [PubMed: 26262553]

[23]. Liu J, Liu Y, Wang Y, Zhu J, Yu J, Hu Z, Mater. Today Commun 2017, 13, 282.

[24]. Zhang J, Wu C, Xu Y, Chen J, Ning N, Yang Z, Guo Y, Hu X, Wang Y, ACS Appl. Mater. Interfaces 2020, 12, 40990. [PubMed: 32808753]

[25]. Pei Z, Yu Z, Li M, Bai L, Wang W, Chen H, Yang H, Wei D, Yang L, Int. J. Biol. Macromol 2021, 179, 324. [PubMed: 33684432]

[26]. Wei D, Wang H, Zhu J, Luo L, Huang H, Li L, Yu X, Macromol. Mater. Eng 2020, 305, 2000018.

[27]. Poonam K Sharma A Aroraa SK Tripathi Journal of Energy Storage 2019, 21, 801.

[28]. Ji Z, Wang H, Chen Z, Wang P, Liu J, Wang J, Hu M, Fe J, Nie N, Huang Y, Energy Storage Materials 2020, 28, 334.

[29]. Liu J, Long J, Shen Z, Jin X, Han T, Si T, Zhang H, Adv. Sci 2021, 8, 2004689.

[30]. Wu Z, Chen J, Boukhvalov DW, Luo Z, Zhu L, Shi Y, Nano Energy 2021, 85, 105990.

[31]. Zhu Y, Sun F, Jia C, Zhao T, Mao Y, Nanomaterials 2022, 12, 104.

[32]. Brooke R, Wijeratne K, Hübscher K, Belaineh D, Ersman PA, Adv. Mater. Technol 2022, 7, 2101665.

[33]. Yu S, Zhang J, Zhu X, Yin Y, Xue J, Xia F, Li Y, Xue Q, Compos. Sci. Technol 2022, 218, 109191.

[34]. Jiang Y, Liang F, Li H, Li X, Fan Y, Cao J, Yin Y, Wang Y, Wang Z, Zhu G, ACS Nano 2022, 16, 746. [PubMed: 34985244]

[35]. Xie M, Zhou Y, Wang Z, Wang H, Yan D, Han B, Zhang S, Deng C, Chem. Eng. J 2022, 431, 133920.

[36]. Park YG, Lee GY, Jang J, Yun S, Kim E, Park JU, Adv. Healthcare Mater 2021, 10, 2002280.

[37]. Wang Z, Xia X, Zhu M, Zhang X, Liu R, Ren J, Yang J, Li M, Jiang J, Liu Y, Adv. Funct. Mater 2021, 32, 2108336.

[38]. Kim MG, Kim C, Alrowais H, Brand O, Adv. Mater. Technol 2018, 3, 1800061.

[39]. Zhang M, Li G, Huang L, Ran P, Huang J, Yu M, Yuqian H, Guo J, Liu Z, Ma X, Applied Materials Today 2021, 22, 100903.

[40]. Guo R, Sun X, Yuan B, Wang H, Liu J, Adv. Sci 2019, 6, 1901478.

[41]. Plevachuk Y, Sklyarchuk V, Eckert S, Gerbeth G, Novakovic R, J. Chem. Eng. Data 2014, 59, 757.

[42]. Liu S, Yuen MC, White EL, Boley JW, Deng B, Cheng GJ, Kramer-Bottiglio R, ACS Appl. Mater. Interfaces 2018, 10, 28232. [PubMed: 30045618]

[43]. Chambel A, Sanati AL, Lopes PA, Nikitin T, Fausto R, Almeida AT, Tavakoli M, Adv. Mater. Technol 2021, 7, 2101238.

[44]. Watson AM, Cook AB, Tabor CE, Adv. Eng. Mater 2019, 21, 1900397.

[45]. Choi YY, Ho DH, Cho JH, ACS Appl. Mater. Interfaces 2020, 12, 9824. [PubMed: 31985196]

[46]. Neumann TV, Dickey MD, Adv. Mater. Technol 2020, 5, 2000070.

[47]. Guo R, Cui B, Zhao X, Duan M, Sun X, Zhao R, Sheng L, Liu J, Lu J, Materials Horizons. 2020, 7, 1845.

[48]. Guo R, Sun X, Yao S, Duan M, Wang H, Liu J, Deng Z, Adv. Mater. Technol 2019, 4, 1900183.

[49]. Kim MS, Kim S, Choi J, Kim S, Han C, Lee Y, Jung Y, Park J, Oh S, Bae BS, Lim H, Park I, ACS Appl. Mater. Interfaces 2022, 14, 1826. [PubMed: 34931517]

[50]. Shi C, Zou Z, Lei Z, Zhu P, Zhang W, Xiao J, Sci. Adv 2020, 6, eabd0202.

[51]. Guo R, Tang J, Dong S, Lin J, Wang H, Liu J, Rao W, Adv.Mater. Technol. 2018, 3, 1800265.

[52]. Chen H, Wang L, Hu B, Xu J, Liu X, Chemosphere 2022, 289, 133182. [PubMed: 34883131]

[53]. Lin S, Ali MU, Zheng C, Cai Z, Wong MH, J. Hazard. Mater 2022, 426, 127792. [PubMed: 34802823]

[54]. N Yi Y Gao, A. L. V. Jr, J Zhu, D. Erdely, C. Xue, R. Lavelle, H. Cheng, Mater. Today 2021, 50, 24.

[55]. Zhang W, Zhang L, Liao Y, Cheng H, Int. J. Extrem. Manuf 2021, 3, 042001.

[56]. Xu S, Zhang Y, Cho J, Lee J, Huang X, Jia L, Fan JA, Su Y, Su J, Zhang H, Cheng H, Lu B, Yu C, Chuang C, Kim T, Song T, Shigeta K, Kang S, Dagdeviren C, Petrov I, Braun PV, Huang Y, Paik U, Rogers JA, Nat. Commun 2013, 4, 1543. [PubMed: 23443571]

[57]. Kang J, Son D, Vardoulis O, Mun J, Matsuhisa N, Kim Y, Kim J, Tok JB, Bao Z, Adv. Mater. Technol 2019, 4, 1800417.

[58]. Liu J, Jiang S, Xiong W, Zhu C, Li K, Huang Y, Adv. Funct. Mater 2021, 32, 2109214.

[59]. Wang H, Liu H, Cao Z, Li W, Huang X, Zhu Y, Ling F, Xu H, Wu Q, Peng Y, Yang B, Zhang R, Kessler O, Huang G, Wu J, PNAS 2020, 117, 11299. [PubMed: 32381742]

[60]. Zhang F, Li H, Cui Y, Li G, Guo Q, AIP Advanced 2018, 8, 045112.

[61]. Awaja F, Gilbert M, Kelly G, Fox B, Pigram P, Prog. Polym. Sci 2009, 34, 948.

[62]. Zolfaghari N, Khandagale P, Ford MJ, Dayal K, Majidi C, The Royal Society of Chemistry 2020, 16, 8818.

[63]. Lan J, Zhou B, Yin C, Weng L, Ni W, Shi L, Polymer 2021, 231, 124111.

[64]. Liang J, Tong K, Pei Q, Adv. Mater 2016, 28, 5986. [PubMed: 27159406]

[65]. Wang J, Cai G, Li S, Gao D, Xiong J, Lee PA, Adv. Mater 2018, 30, 1706157.

[66]. Thrasher C, Farrel Z, Morris N, Willey C, Tabor C, Adv. Mater 2019, 31, 1903864.

[67]. Matsuhisa N, Inoue D, Zalar P, Jin H, Matsuba Y, Itoh A, Yokota T, Hashizume D, Someya T, Nat. Mater 2017, 16, 834. [PubMed: 28504674]

[68]. Song P, Qin H, Gao H, Cong H, Yu S, Nat. Commun 2018, 9, 2786. [PubMed: 30018323]

[69]. Zhu H, Wang S, Zhang M, Li T, Hu G, Kong D, npj Flexible Electron. 2021, 5, 25.

[70]. Zhang F, Ren D, Huang L, Zhang Y, Sun Y, Liu D, Zhang Q, Feng W, Zheng Q, Adv. Funct. Mater 2021, 31, 2107082.

[71]. Lopes PA, Santos BC, Almeida AT, Tavakoli M, Nat. Commun 2021, 12, 4666. [PubMed: 34344880]

[72]. Lopes PA, Fernandes DF, Silva AF, Marques DG, Almeida AT, Majidi C, Tavakoli M, ACS Appl. Mater. Interfaces 2021, 13, 14552. [PubMed: 33689286]

[73]. Bae TW, Kwon KK, ECG PQRST complex detector and heart rate variability analysis using temporal characteristics of fiducial points. Biomed. Signal Process. Control 2021, 66, 102291.

[74]. Nigusse AB, Malengier B, Mengistie DA, Tseghai GB, V Langenhove L, Sensors 2020, 20, 6233. [PubMed: 33142899]

[75]. Kim S, Jeon H, Shin S, Park S, Jegal J, Hwang S, Oh DX, Park J, Adv. Mater 2018, 30, 1705145.

[76]. Zhang L, Liu Z, Wu X, Guan Q, Chen S, Sun L, Guo Y, Wang S, Song J, Jeffries EM, He C, Qing F, Bao X, You Z, Adv. Mater 2019, 31, 1901402.

[77]. Guo W, Wang X, Lu X, Li X, Li Y, Sun J, ACS Appl. Polym. Mater 2019, 7, 21927.

[78]. Wang H, Yang Y, Nishiura M, Higaki Y, Takahara A, Hou Z, J. Am. Chem. Soc 2019, 141, 3249. [PubMed: 30727726]

[79]. Jang K, Chung H, Xu S, Lee CH, Luan H, Jeong J, Cheng H, Kim GT, Han SY, Lee JW, Kim J, Cho M, Miao F, Yang Y, Jung HN, Flavin M, Liu H, Kong GW, Yu KJ, Rhee S, Chung J, Kim B, Kwak JW, Yun MH, Kim JY, Song YM, Paik U, Zhang Y, Huang Y, J, A. Rogers, Nat. Commun 2015, 6, 6566. [PubMed: 25782446]

[80]. Long Y, Wei H, Li J, Yao G, Yu B, Ni D, Gibson AL, Lan X, Jiang Y, Cai W, Wang X, ACS Nano 2018, 12, 12533. [PubMed: 30488695]

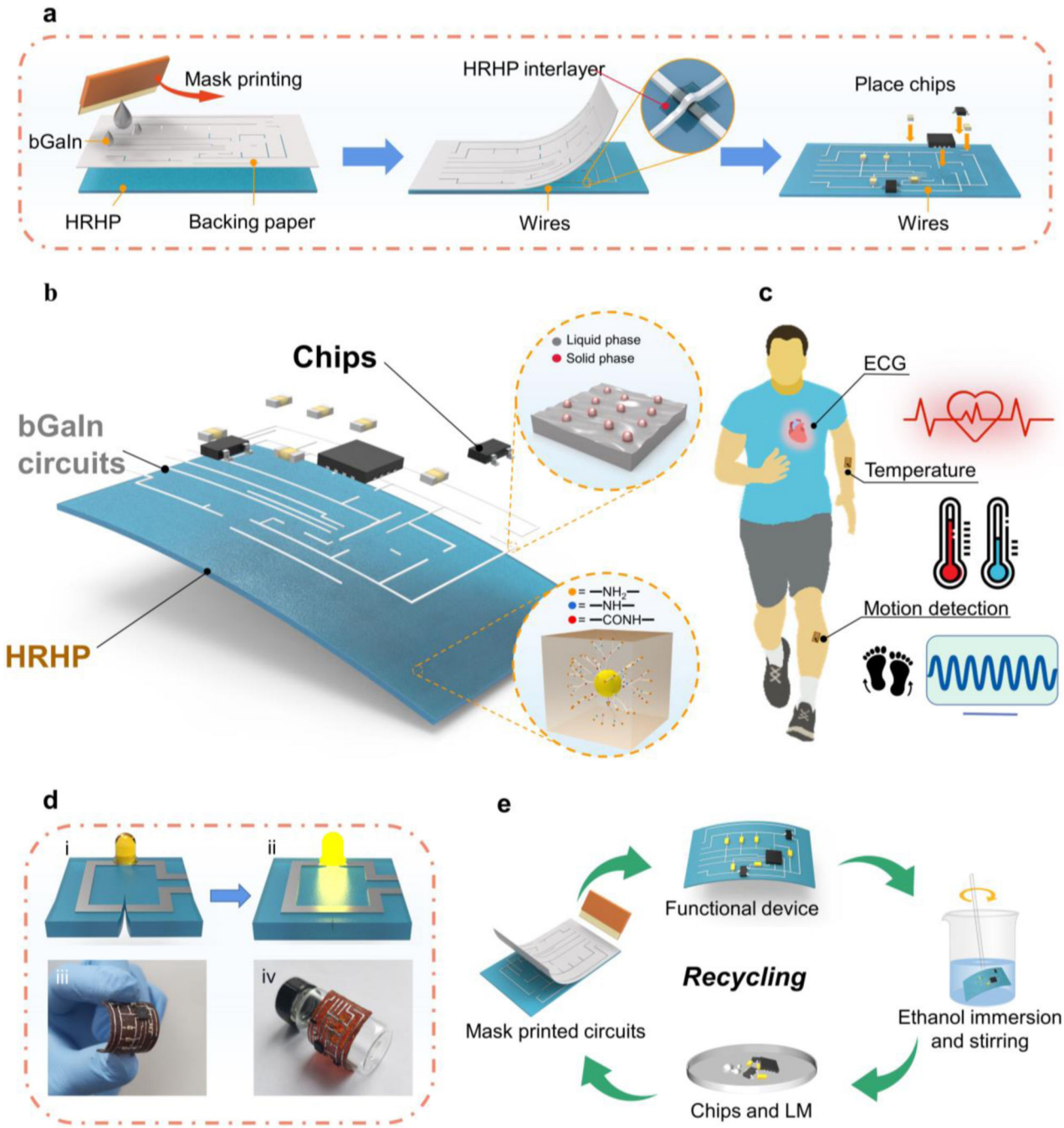

Figure 1. Design and demonstration of flexible, self-healing, recyclable multifunctional wearable electronics.

(a) Schematic showing the fabrication process. (b) Exploded view of proof-of-the-concept multifunctional electronics to monitor (c) electrophysiology, temperature, and motions. (d) (i, ii) Schematic showing the self-healing characteristics and (iii, iv) its mechanical robustness against bending after healing. (e) Recycling of liquid metal and chips for reuse in fabricating new self-healing electronics.

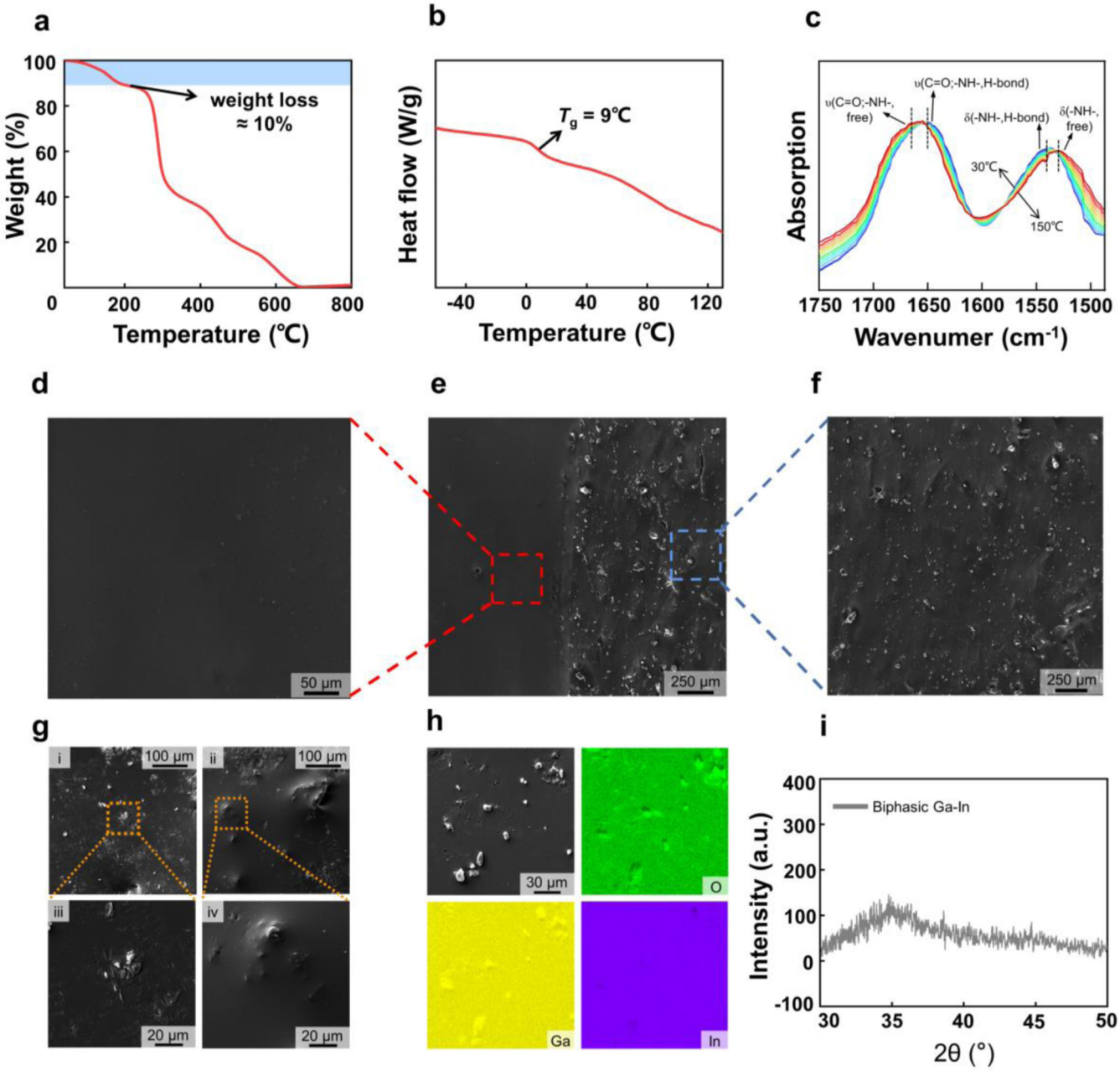

Figure 2. Characterization of HRHP and bGaIn.

(a) TGA curve of HRHP heated from 25 to 800°C. (b) DSC thermogram of HRHP heated from −65 to 130°C at a rate of 10°C min^{-1}. (c) Temperature-dependent FTIR spectra of HRHP upon heating from 30 to 150°C. (d) SEM of HRHP film surface before CO_2 laser ablation. (e) SEM picture of HRHP surface before (left) and after (right) CO_2 laser ablation (CO_2 laser parameters: grating mode, power 35%, speed 100%). (f) SEM of HRHP film surface after laser CO_2 ablation. (g) SEM images of the bGaIn, iii and iv are the partially enlarged pictures of i and ii, respectively. (h) Energy dispersive spectroscopy mappings of bGaIn, the solid particle region shows a high oxygen and gallium concentration. (i) X-ray diffraction patterns of the bGaIn.

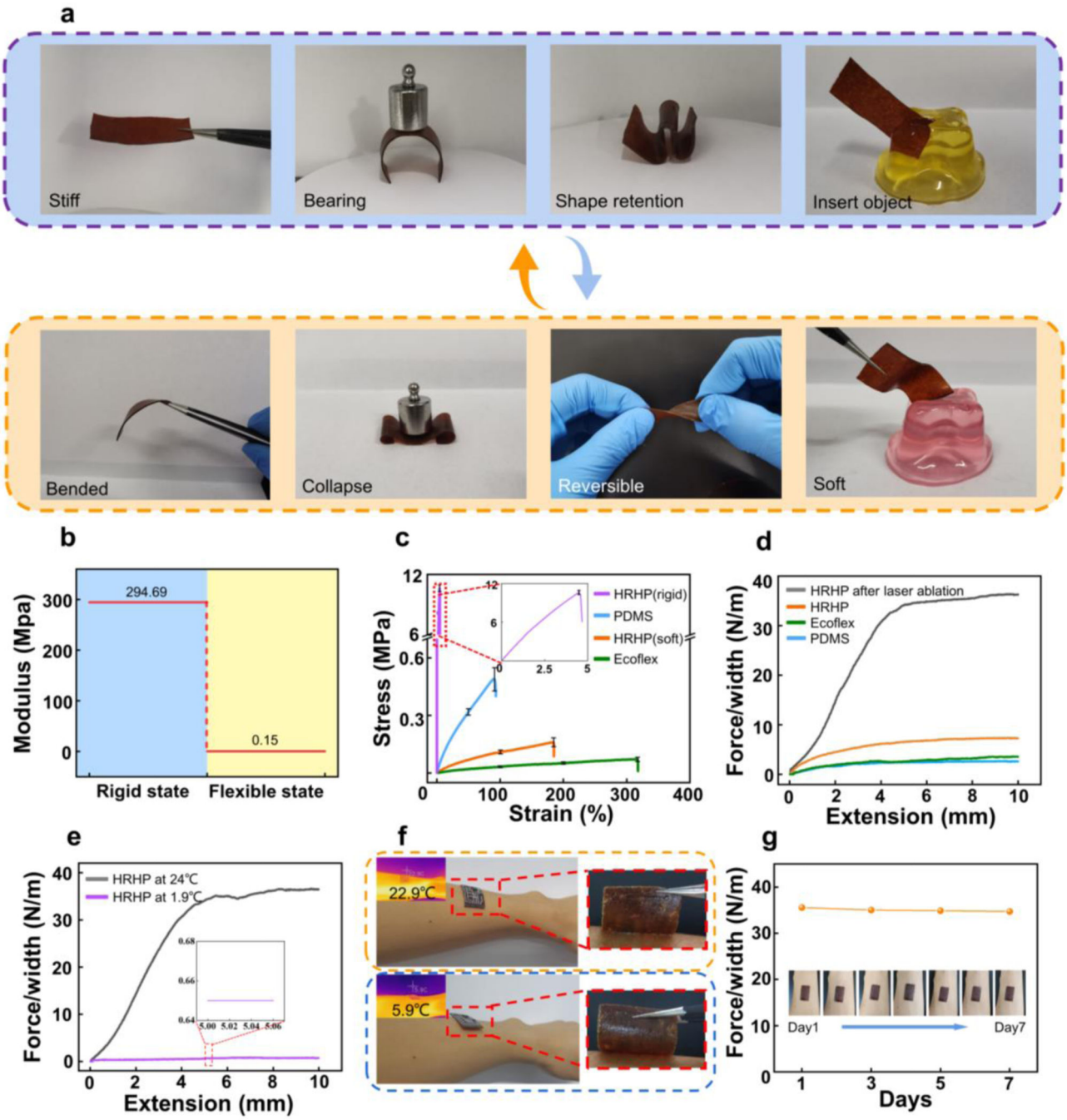

Figure 3. Characterization of mechanical properties and adhesion of HRHP films.

(a) Demonstration of the variable stiffness of the HRHP film in rigid (top) and flexible (bottom) states. (b) The elastic modulus of HRHP decreases from 294.69 MPa to 0.15 MPa as it switches from a glassy to a rubbery state. (c) The stress-strain curves of HRHP (flexible), HRHP (rigid), PDMS, and Ecoflex. (d) The measured adhesion of PDMS, Ecoflex, pristine HRHP, and HRHP after laser ablation (grating mode, power 35%, speed 100%). (e) The comparison in adhesion of HRHP at 24°C and 1.9°C. (f) Optical and infrared

images of HRHP strongly adhered to the skin at 22.9°C and easily removed at 5.9°C. (g) The durability test of the strong adhesion of the flexible HRHP on the skin over a week.

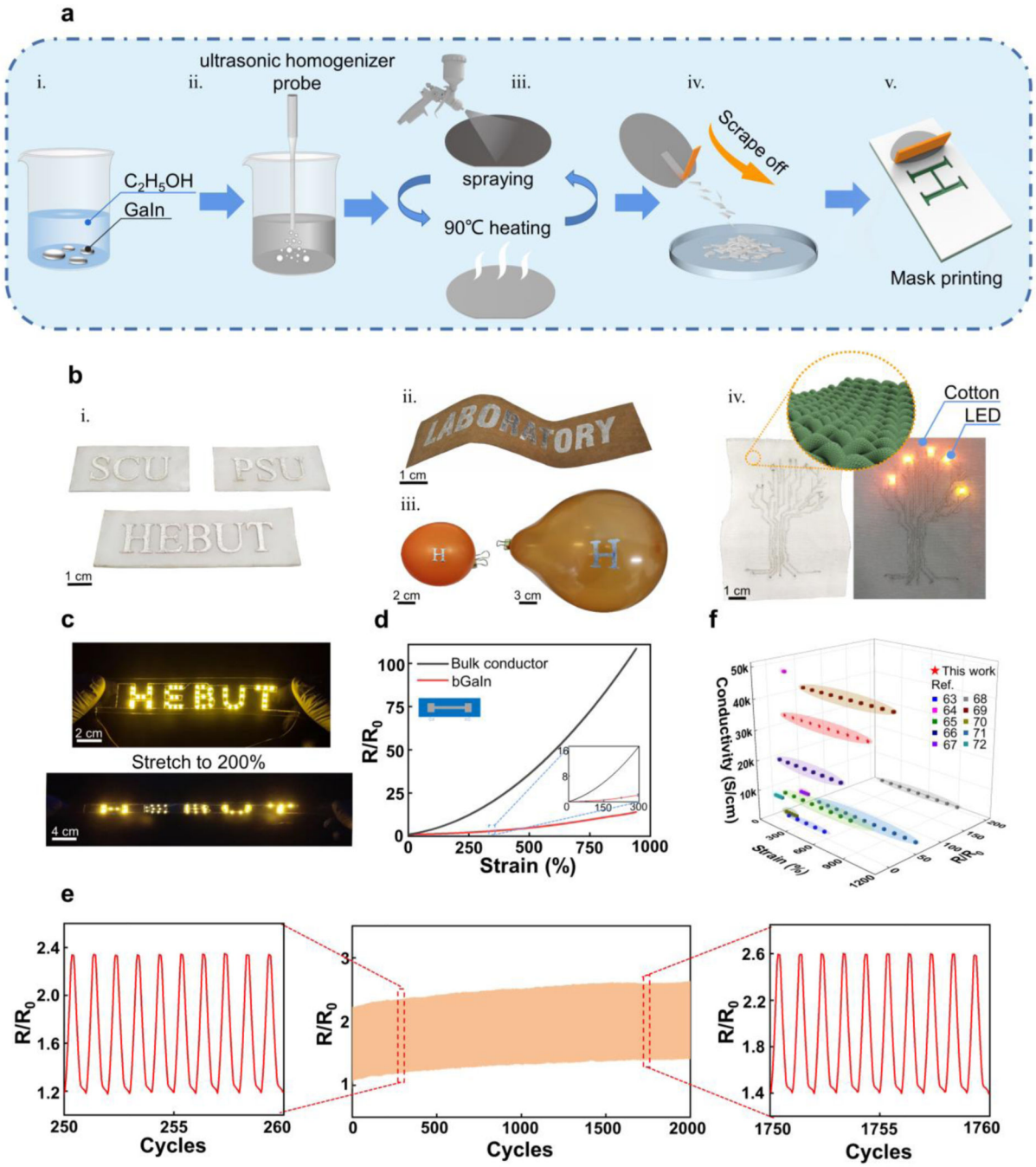

Figure 4. Electromechanical characterizations of bGaIn.

(a) Schematic showing the fabrication process of bGaIn: (i) GaIn mixed with ethanol was first treated with (ii) a ultrasonic homogenizer to obtain uniform GaIn ink. (iii) After repeated spraying GaIn ink on a Si wafer and drying at 90°C, (iv) scraping off the material yielded the bGaIn paste for (v) printing bGaIn patterns through a shadow mask. (b) Printed bGaIn patterns on (i) VHB tape (scale bar, 1 cm), (ii) kraft paper (scale bar, 2 cm), (iii) the surface of a latex balloon, and (iv) cotton fiber with LEDs (scale bar, 1 cm). (c) The LED array with a “HEBUT” pattern before and after a tensile strain of 200%. (d) Normalized

resistance change of the bGaIn traces on VHB tape with the tensile strain up to 940% (error bars from five samples), with the inset to 300% (black lines: theoretical predictions based on bulk liquid metal conductors). (e) The stability testing of the bGaIn traces on VHB over 2,000 cycles to 300% stretching. (f) Comparison of initial conductivity, stretchability, and normalized resistance change at maximum strain between bGaIn from this work and other stretchable conductors.

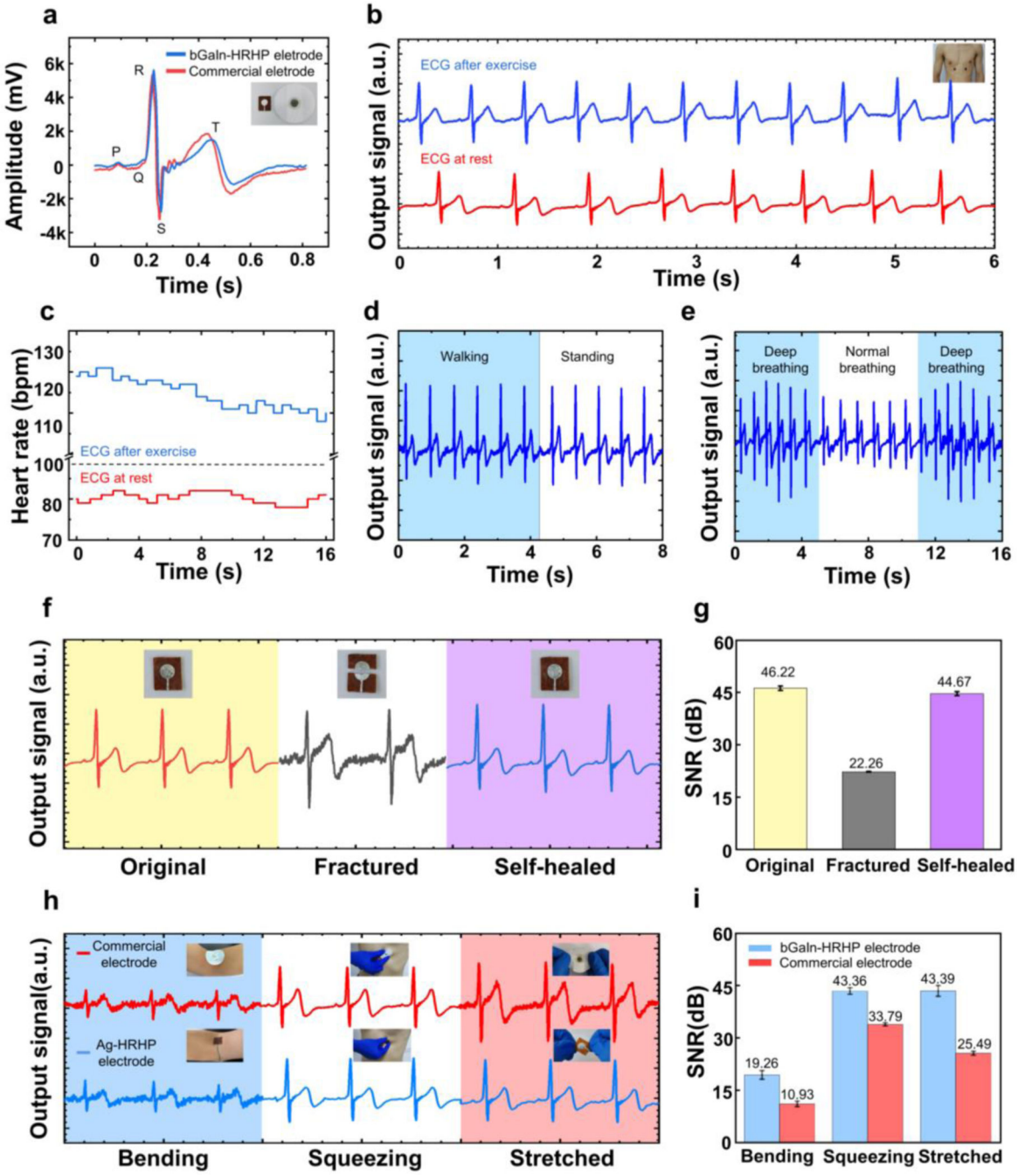

Figure 5. Application of self-healing electrodes for motion artifact-free ECG detection.

(a) Comparison of ECG signals between bGaIn-HRHP and commercial electrodes. (b) ECG signals and (c) heart rate detected by bGaIn-HRHP electrodes after exercise and at rest. (d) ECG signals measured during continuous walking and followed by standing. (e) ECG signals measured under normal breathing and deep breathing with lowered S peaks. (f) ECG signals collected from the bGaIn-HRHP electrode in the original, fractured, and self-healed state, as well as (g) the corresponding SNR values. (h) Comparison of the ECG signals

between the bGaIn-HRHP and commercial electrodes upon elbow bending, chest squeezing, and stretching, with (i) the corresponding SNR values.

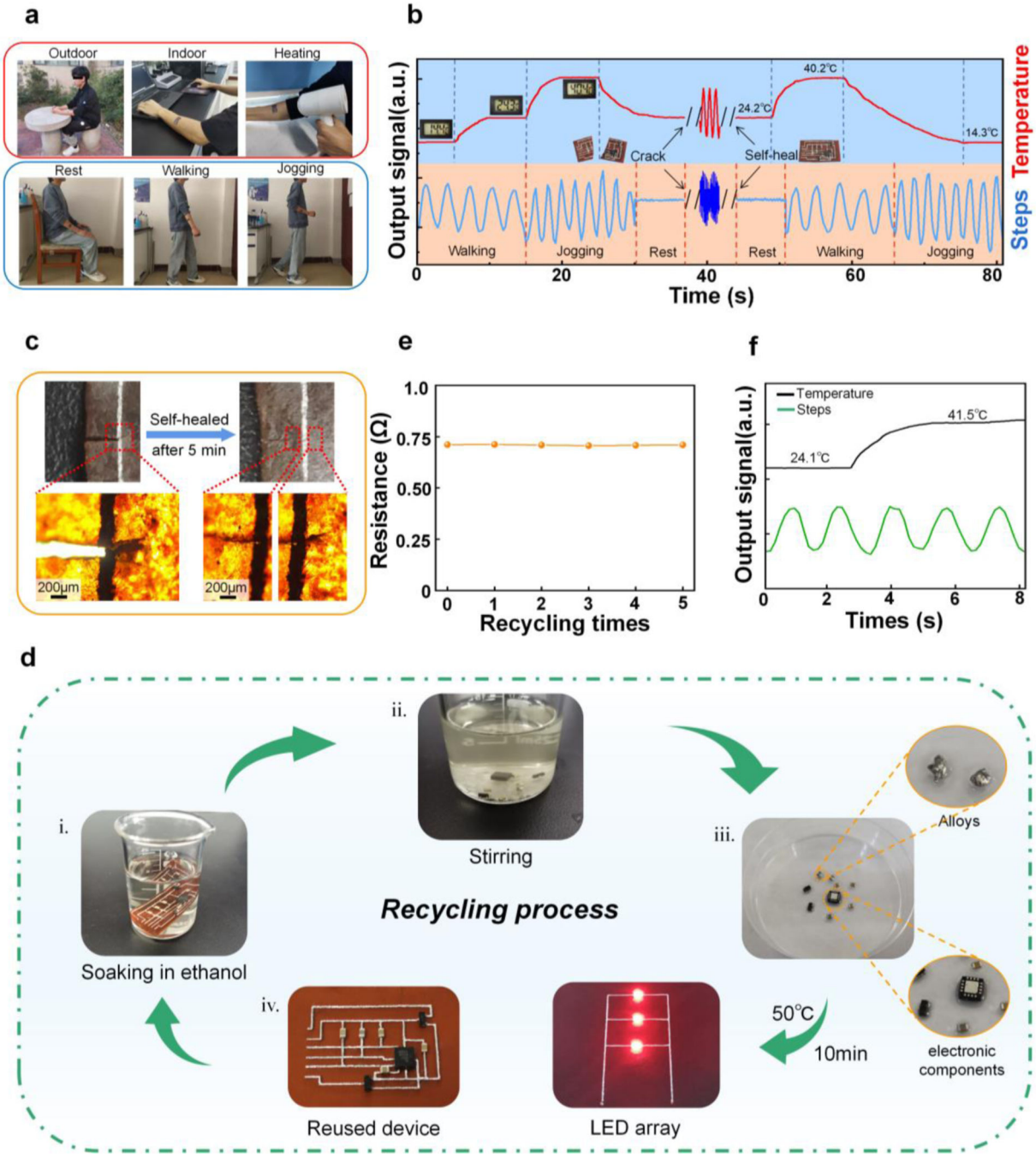

Figure 6. Application of recyclable bGaIn and COTS components on temperature-switching HRHP with variable stiffness characteristics for multifunctional devices.

(a) Demonstration of the device platform attached to the arm to detect temperature and varying motion in different activities, with (b) the signals (temperature in red and motion in blue) measured before fracture, upon fracture, and after self-healing. (c) Image showing the self-healing process of the multifunctional device. (d) The recycling process of bGaIn and electronic components starts with (i) soaking of the device in ethanol and (ii) stirring with a glass rod to separate them from the substrate. (iii) Drying at 50°C for 10 minutes yields (iv) the recycled bGaIn and electronic components for reuse. (e) Comparison of the resistance of

the bGaIn recycled from zero to five times. (f) Demonstration of the new device prepared by the recycled bGaIn and electronic components for detecting temperature and motion.

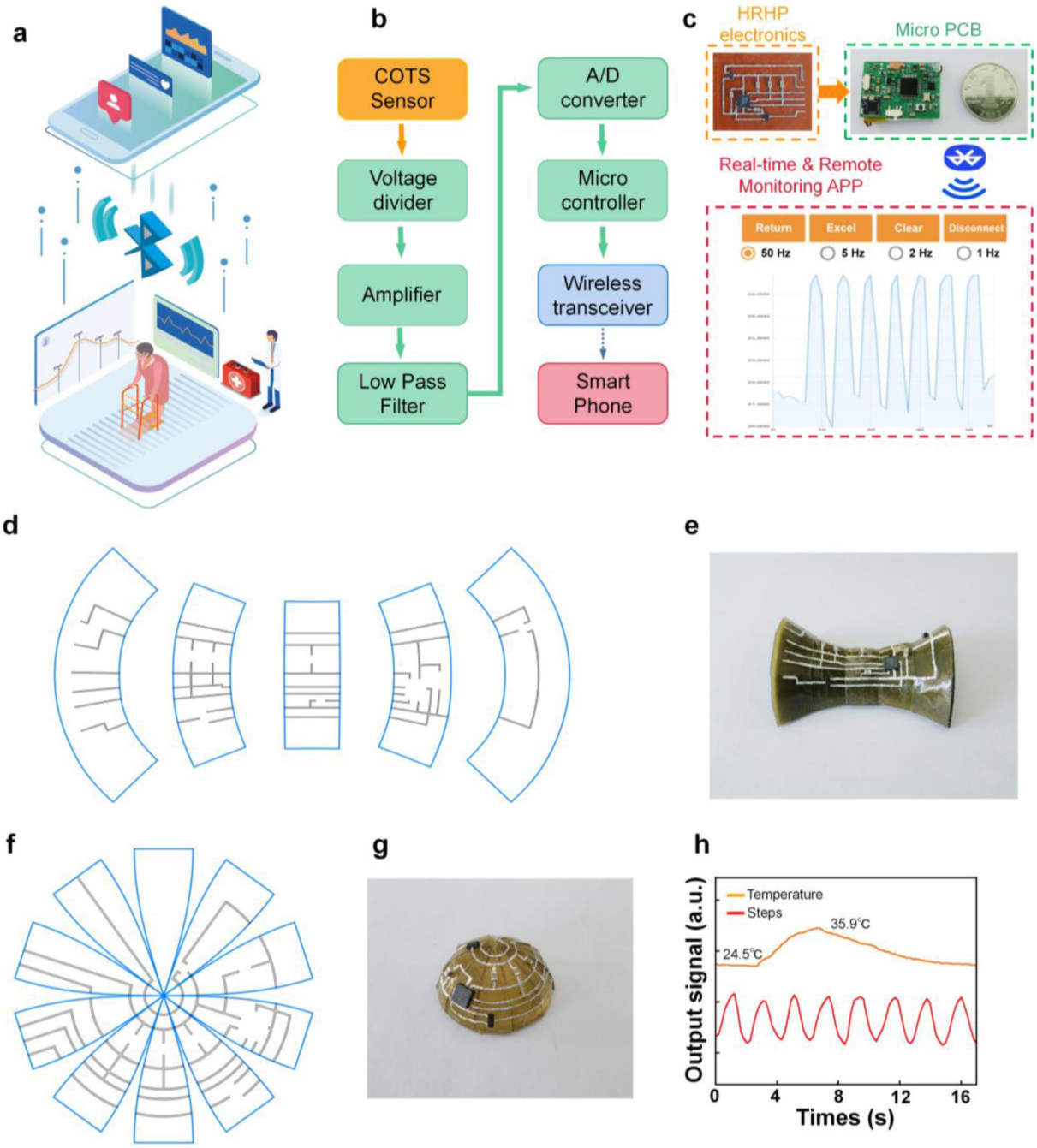

Figure 7. Integrated system for remote motion monitoring and conformal electronics based on 3D self-assembly.

(a) Schematic illustrations and (b) block diagram of the integrated remote monitoring platform. (c) Photograph to show each module in the integrated remote monitoring system. (d,f) Design of the 2D parts for (e,g) self-assembled devices on the (d,e) saddle and (f,g) hemispherical surfaces. (h) Detection of temperature and motion from the conformal device on the saddle surfaces.